01 Jan 2003

# Analysis of Photobioreactors for Culturing High-Value Microalgae and Cyanobacteria Via an Advanced Diagnostic Technique: CARPT

Hu Ping Luo

Abdenour Kemoun

Muthanna H. Al-Dahhan
*Missouri University of Science and Technology*, aldahhanm@mst.edu

J. M.Fernández Sevilla

*et. al. For a complete list of authors, see https://scholarsmine.mst.edu/che_bioeng_facwork/1348*



## Recommended Citation

H. P. Luo et al., "Analysis of Photobioreactors for Culturing High-Value Microalgae and Cyanobacteria Via an Advanced Diagnostic Technique: CARPT," *Chemical Engineering Science*, vol. 58, no. 12, pp. 2519 - 2527, Elsevier, Jan 2003.
The definitive version is available at https://doi.org/10.1016/S0009-2509(03)00098-8

PERGAMON

Chemical Engineering Science 58 (2003) 2519–2527

Chemical Engineering Science

www.elsevier.com/locate/ces

# Analysis of photobioreactors for culturing high-value microalgae and cyanobacteria via an advanced diagnostic technique: CARPT

Hu-Ping Luo[a,*], Abdenour Kemoun[a], Muthanna H. Al-Dahhan[a], J. M. Fernández Sevilla[b], J. L. García Sánchez[b], F. García Camacho[b], E. Molina Grima[b]

[a] *Chemical Reaction Engineering Laboratory (CREL), Department of Chemical Engineering, Washington University, One Brookings Drive, Campus Box 1198, St. Louis, MO, 63130-4899, USA*

[b] *Department of Chemical Engineering, University of Almería, Spain*

Received 1 October 2002; received in revised form 3 December 2002; accepted 18 December 2002

**Abstract**

Photosynthetic algal cultures are a potential source of many high-value products. In photobioreactors (PBR), the availability and the intensity of the light, which are affected by the cells' movement, are the major factors controlling the biomass productivity. Hydrodynamics, hence, play a significant role in the reactor's performance, as they determine not only the flow field, i.e. liquid flow and mixing, shear stresses, etc., but also the movements of the cells. In this work, computer-automated radioactive particle tracking (CARPT) technique was employed to evaluate its feasibility for characterizing PBRs. Liquid velocity profiles, cells' movement, and the temporal irradiance patterns obtained by coupling the cells' trajectories and the irradiance distribution model have been determined. The effects of the biomass concentration, reactor geometry, and the aeration rate on the irradiance patterns are discussed. The results demonstrate that the CARPT technique is promising for PBR analysis. It provides fundamental information needed to advance the cells' growth prediction and modeling, and the design, scale-up and operation of PBRs.


*Keywords:* Photobioreactor; CARPT; Hydrodynamics; Bubble column; Airlift

## 1. Introduction

Microalgae and cyanobacteria are photosynthetic organisms and sources of many high-value products (Becker, 1994; Vonshak, 1992), such as polyunsaturated fatty acids (PUFAs), antiviral agents (e.g., red antiviral polycaccharides (RMP) and anti-herpes agent), natural, environment-friendly compounds for combating plant pathogens, e.g., antifungal agents (Kulick, 1995), and pigments (natural food colorants and fluorescence indicator bind to antibodies for use in clinical and research immunoassays). Growing interesting microalgae and cyanobacteria for these products requires protecting them from the exterior environment and hence they are cultured in closed axenic photobioreactors, e.g., airlift, bubble column, and tubular reactors, in which the operational variables are completely controllable.

In PBRs, the availability and intensity of light are the major factors controlling the biomass productivity of these photosynthetic cultures. Light intensity decreases sharply with distance from the illuminated surface, especially in the case of dense cultures and strong external irradiance, which are a must for economic operation of the closed PBRs. The cells near the reactor wall experience a high photon flux density that causes photoinhibition (Barber & Andersson, 1992), while the cells elsewhere in the reactor experience very low photon flux (darkness) that causes photolimitation. It is well known that both the quantity and the quality of the light delivered to the cells are significant to the cells' growth (Pulz & Scheibenbogen, 1998; Markl, 1980; Laws, Terry, Wichman, & Chalup, 1983; Merchuk, Ronen, Giris, & Arad, 1998). In other word moving the cells in and out of the optimally illuminated zones at suitable frequencies can improve productivity. Hence, the biomass productivity and the performance of the PBRs depend greatly on the cells' movement as well as on the transport parameters, the photosynthetic kinetics and the irradiance characteristics.

* Corresponding author. Tel.: +1-314-935-6042; fax: +1-341-935-7211.

*E-mail address:* hpluo@wuche.che.wustl.edu (H.-P. Luo).

0009-2509/03/$ - see front matter © 2003 Elsevier Science Ltd. All rights reserved.
doi:10.1016/S0009-2509(03)00098-8

The cells' movement is controlled by the reactor hydrodynamics and the flow patterns inside the reactor, i.e. the liquid flow and mixing, shear stresses, gas holdups, etc. Although substantial work exists on the culturing of phototrophs, both flow patterns and their effects on the overall performance of PBRs remain unclear. As a consequence, most of the work (Aiba, 1982; Grima, Camacho, Peres, Fernandez, & Sevilla, 1997; Rorrer & Mullikin, 1999) is empirical and applied to specific processes. For example, the current models for the performance prediction of PBRs, based on static photosynthetic growth rate models, take into account only the volume averaged irradiance doses and disregard the dynamic nature of the system or how light is delivered to the cells. Given these limitations, the design and scale-up of PBRs for the growth of phototrophic culture requires extensive, costly, and labor-intensive empirical developmental efforts.

Accordingly, there is a need for a fundamentally based modeling approach that integrates the principles of hydrodynamics, the irradiance field, and photosynthesis to enhance biomass productivity by maximizing growth rate and efficiency in light use. This approach requires in-depth knowledge and proper understanding of both photosynthetic growth and flow dynamics inside the bioreactor. Unfortunately, most traditional experimental techniques, e.g., Pitot tube, laser doppler anemometry, particle image velocimetry, etc., cannot provide such knowledge because they are incapable of being used in either multiphase systems or in opaque systems.

Computer-automated radioactive particle tracking (CARPT), an advanced non-invasive diagnostic technique, has been used extensively and successively in characterizing the flow field in multiphase reactors (Devanathan, Moslemian, & Dudukovic, 1990; Degaleesan, 1997; Roy, Larachi, Al-Dahhan, & Dudukovic, 2002; Kumar and Dudukovic, 1997). CARPT has been used to measure multiphase flow field, liquid velocity, trajectory distribution, and turbulence parameters.

This work demonstrates the feasibility of CARPT in characterizing the cells' movements and the irradiance intensity pattern in PBRs. Traditional hydrodynamic parameters, as well as information about cell movements, represented by particle Lagrangian trajectory, were obtained in two airlift bioreactors (draft tube and split columns). In addition, selected CARPT data from our databank on bubble columns is also employed for analysis. The information has been used to evaluate the possible irradiance patterns (i.e., the light history of the cells) that would be obtained with different biomass concentrations.

## 2. The CARPT technique

In principle, the CARPT technique measures the flow field by tracking a small radioactive particle that is made specifically to follow the interested phase in the reactors. In order to have the particle follow the motion of the liquid phase or the liquid element in the reactor precisely, it is prepared to be fully wettable and neutrally buoyant, i.e., its density is equal to or very close to the density of the liquid phase. In this case, the particle is usually a composite made by inserting a certain mass of SC-46 (which emits $\gamma$-rays with an activity of 50–500 μCi) into a hollow polypropylene particle of diameter 0.8–2.3 mm. Buoyancy is adjusted by injecting additional non-radioactive material into the internal void. However, for monitoring the flow of solids in gas–liquid–solid, liquid–solid, and gas–solid systems, a radioactive particle of the same density, size (the diameter can be as low as 100–150 μm) and shape as the solids phase is used.

The instantaneous particle position is identified by monitoring simultaneously the radiation intensities at a set (16–32) of sodium iodide (NaI) detectors located strategically around the column, as shown in Fig. 1. The radiation intensity recorded at each detector decreases exponentially with increasing distance between the particle and the detector. In order to reconstruct properly the position of the particle from radiation intensities, calibration needs to be performed prior to the CARPT experiment. While the reactor is operated at the same conditions of the CARPT experiment, the particle is placed at many known locations ($\sim$ 500–3000 known positions; depending on the reactor size) and the radiation recorded by each detector is monitored. Using the acquired information, calibration curves are established that relate the intensity received at a detector to the distance between the particle and the detector. Thereby, a sequence of instantaneous position data is obtained that yields the position of the particle at successive sampling instants (i.e., its trajectory). Recently, the resolution of the technique has been improved to be within 1–2 mm.

Differentiation of the data yields particle instantaneous velocities. Each evaluated velocity is assigned to a fictitious compartment in the 3-D reactor domain at the middle distance between two successive locations. Ensemble averaging of the velocities in each compartment yields the time averaged quantities and the spatial flow field for the whole column. The instantaneous and time averaged velocities can then be used to determine fluctuating velocity and hence various turbulence parameters (Reynolds stresses, turbulent kinetic energy, turbulent eddy diffusivities, etc.). The hardware and software developed for the CARPT technique and its data processing are described elsewhere (Degaleesan, 1997; Roy et al., 2002).

The accuracy of determining the fluid element velocity using the particle tracking technique depends in part on the ability of the tracer particle to follow the liquid element. Close matching of the density of the particle with that of the liquid ensures that the particle is neutrally buoyant. However, the finite size of the particle makes it differ from a liquid element and unable to sample small scale eddies. Degaleesan (1997) showed that for a particle of size 2.36 mm, and a difference of 0.01 gm $cm^{-3}$ in density between the particle and the liquid, the maximum difference in the velocity (between particle and liquid) is 1 cm $s^{-1}$. Degaleesan (1997) estimated that the frequency at which the measured

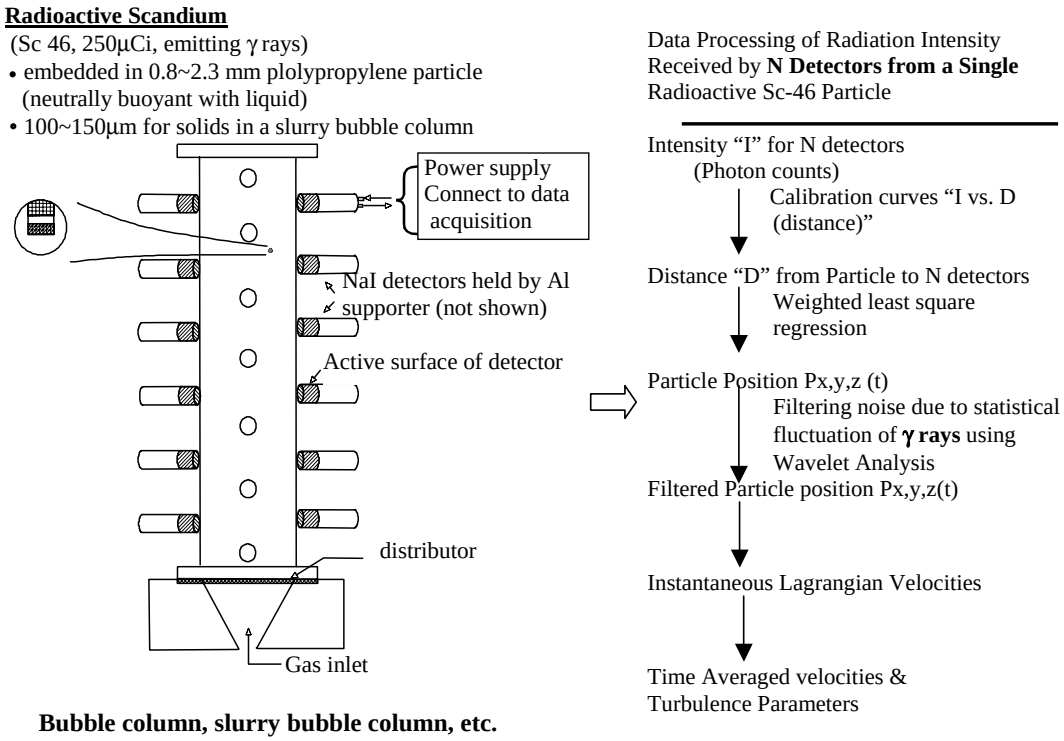


Fig. 1. Schematic diagram of the CARPT facility at the Chemical Reaction Engineering Laboratory (CREL), Washington University (WU).

velocity of a 2.36 mm particle is follow up to 99% of the liquid velocity is 30 Hz and hence she suggested that 50 Hz sampling frequency is sufficient for bubble columns. She also showed that for frequency lower than 30 Hz, which represents the large scale eddies, the particle will be able to closely follow the liquid phase, and the measured particle fluctuating velocities can be considered to be those of the liquid phase. Small scale eddies cannot be followed by such particle. However, smaller radioactive particle ($< 2.36$ mm) enhances the accuracy of its ability to follow fluid elements and eddies with 50 Hz or higher frequencies.

## 3. Experiments

In this work, CARPT experiments have been carried out in two airlift photobioreactors, a draft tube and a split column, to characterize their liquid flow pattern, the cells' movements, and the irradiance pattern. The configurations of the draft tube and the split columns, with their dimensions, are shown in Fig. 2. In the draft tube bioreactor, an internal column was mounted coaxial to the primary cylinder, with bottom clearance of 1 cm. In the split column, a plate was inserted in the center of the column, separating the column into identical cross-sectional areas: a riser zone and a downcomer zone with bottom clearance of 2.3 cm, designed to match the bottom clearance area of the draft tube bioreactor (i.e., the flow area between the riser and the downcomer). Different type of spargers, as shown in Fig. 2, were used to generate rather uniform gas holdup in the aeration zone: a cross sparger was used in the draft tube column, while an 'H' type of sparger was used in the split column. Both of the spargers have 13 upward facing holes of 1 mm diameter, and they were installed 19 cm above the base in the center of the corresponding aeration zone.

In the CARPT experiments, air was bubbled through the sparger into a batch of tap water at room temperature and atmospheric pressure at superficial gas velocities ($U_g$) of 1 and 5 cm $s^{-1}$ to mimic the typical conditions for microalgae and cyanobacteria cultivation processes. The static liquid level in the draft tube and split columns is 165 cm, corresponding to the top of the baffle in both bioreactors. Since the microalgae cells are very small and their density is close to water, the cells can be assumed to fully follow the liquid flow. Hence, a neutrally buoyant radioactive particle of SC 46 with a diameter of 2.3 mm was used to mimic the cells and to characterize the cells' movement at a sampling frequency of 50 Hz. (Since these CARPT experiments were conducted, we have been able to reduce the size to 0.8 mm in diameter.) Calibration was performed a priori for 672 known locations, which were selected to represent all the regions in the whole column. Each experiment was run for 24 h to assure that the number of the tracer particle visits (occurrences) to each reactor compartment was statistically sufficient to confirm that the time averaged liquid velocity had reached plateau. It was found that 50 visits should

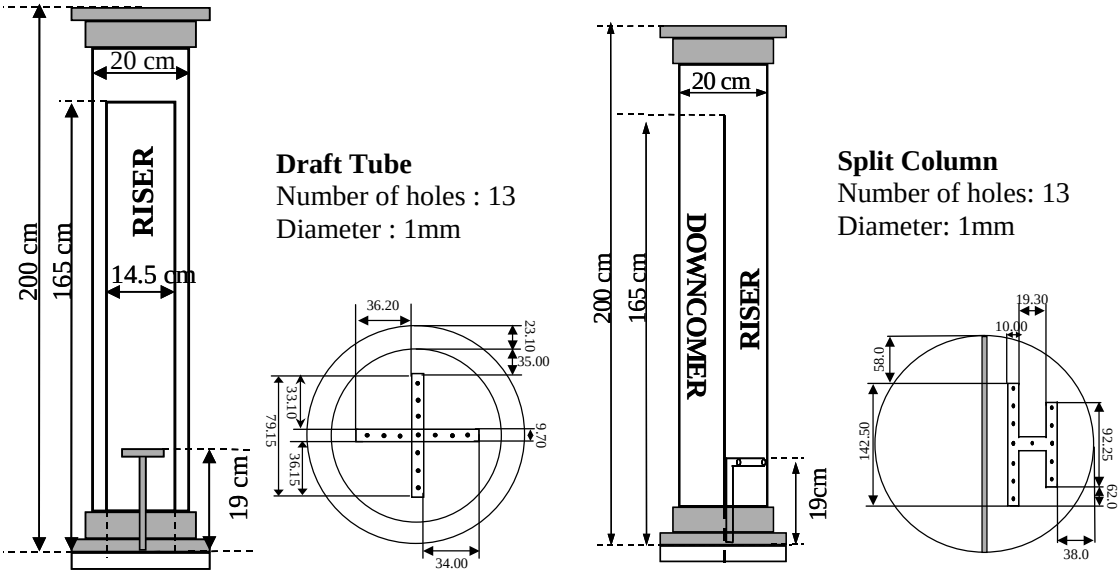


Fig. 2. Configuration of draft tube and split airlift bioreactor.

be enough; however, in these experiments, the number of the particle visits (occurrences) in most compartments was more than 150.

In our laboratory, an extensive databank for CARPT experiments with a 2.3 mm radioactive particle is available for bubble columns of different configurations at operation conditions that cover both bubbly and churn turbulent flow regimes. For a bubble column of diameter 20 cm, the same as that of the airlift reactors used (Fig. 2), CARPT data is available at a superficial gas velocity of 5 cm $s^{-1}$ using a static liquid level of 115 cm and a perforated plate sparger of 0.1% open area and hole diameter of 0.33 mm. This particular set of CARPT data has been also processed to compare the evaluated irradiance patterns in airlift reactors with those obtained in bubble columns without internals at the same operating conditions.

## 4. Results and discussion

### 4.1. Liquid flow field

Instantaneous velocity of the tracer particle is calculated by time-differentiating the successive particle location data obtained from CARPT experiments. To show the overview of the time averaged flow field, the liquid velocities have been time- and ensemble-averaged. The resulting velocity vectors for the draft tube and the split column at $U_g =$ 5 cm $s^{-1}$ are visualized in Fig. 3. For the draft tube column, the time-averaged velocity vectors either have been azimuthally averaged and shown in the $r$–$z$ plane, or have been axially averaged according to the developed flow zone and shown in the cross-sectional plane. While for the split column, due to the asymmetric nature of the geometry and the fluid pattern, two planes in $r$–$z$ plane have been selected to show the velocity vectors in different flow zones: a plane 'along' the split plate (not fully as there is a small angle between them) and a plane 'perpendicular' to the split plate (the two shown planes are exactly perpendicular to each other). In the cross-sectional plane, the velocity vectors have been axially averaged corresponding to the developed flow zone as treated in the draft tube column. The visualization of the flow field clearly shows how the liquid circulates between the riser and the downcomer, and how the liquid elements move in the radial direction. As can be seen, in the cross-sectional plane of the split column, four small eddy vortices are present in the riser and in the downcomer, indicating a possible spiral movement of the liquid elements, which is not observed in the draft tube column. This flow pattern will certainly affect the growth of the cells as the cells circulate from the illuminated surface to the dark center, or in other words experience the so-called light/dark cycle. The time scale for this fluctuation, called type II, is observed to be in the order of 1 s. The length scale for the spiral movement in the radial direction is 10 cm (equivalent to half of the column diameter). It is noteworthy here that, since the vortices are observed in the time-averaged vector plot, the liquid elements may not always follow the spiral movement.

### 4.2. Cell movements

Fig. 4 shows typical Lagrangian trajectories that represent the particle's movement for a single circulation in the reactor obtained from the CARPT experiments at a superficial gas velocity of 1 cm $s^{-1}$ in both the draft tube and the split columns. As mentioned above, the particle trajectories approximate the cells' movement. Since the particle movement has been measured for a long time (24 h) that

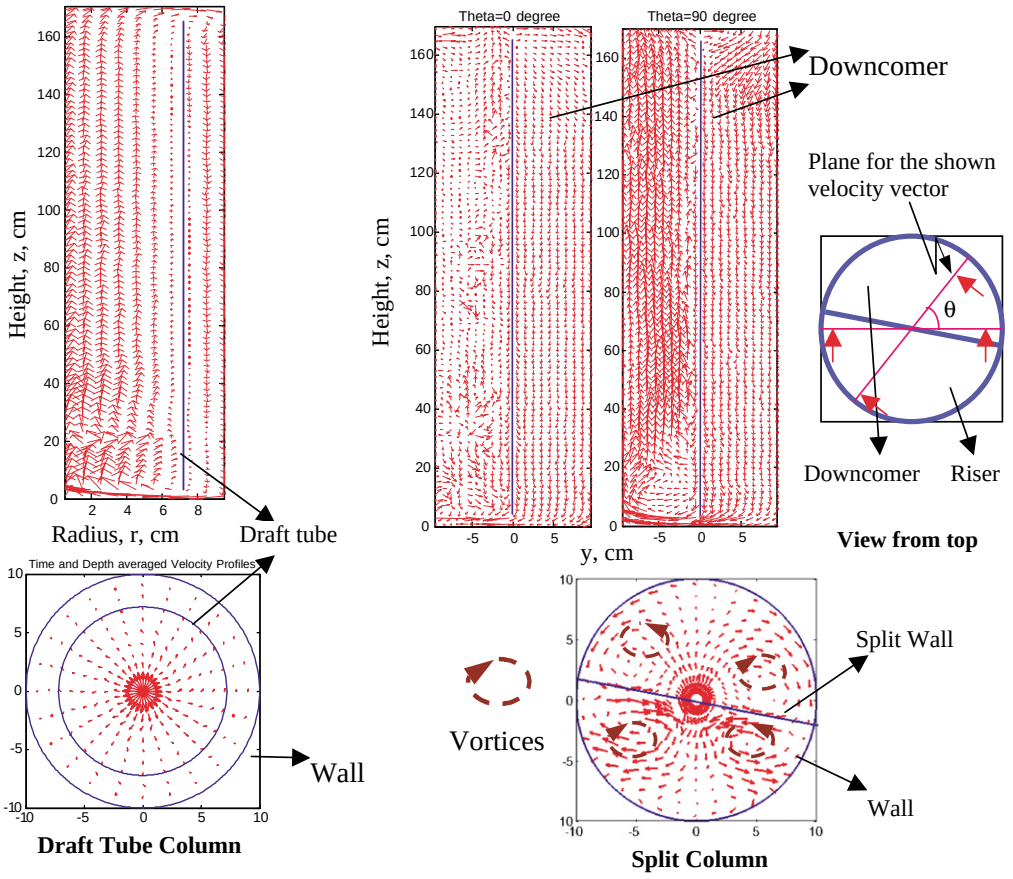


Fig. 3. Visualization of the liquid flow field for draft tube column and split column at $U_g = 5$ cm s$^{-1}$. The time-averaged velocity vectors have been further axially averaged according to the developed flow zone ($z = 0.6 \sim 1.4\,m$) and shown in the cross-sectional plane for both reactors, while only for the draft tube column, the velocity vectors have been azimuthally averaged and shown in the $r$–$z$ plane. Please see the text for details. Arrows present the liquid velocity vectors projected on the shown plane, and the solid lines inside the figures represent the walls and internals (i.e. the draft tube or split wall).

the particle visits any part of the reactor for many times, it is reasonable to assume that the obtained particle trajectories represent the movement of the cells in the reactor. These are the basic information for further analysis of the flow pattern and hydrodynamic parameters.

As expected, the trajectories demonstrate the circulation of the cells between the riser and the downcomer over a time scale of 20 s and length scale of 20 cm in radial direction (equivalent to the diameter of the reactor). In the draft tube column, where the riser is dark but the downcomer is illuminated, this circulation again causes light fluctuation, called type I. Moreover, the trajectories also demonstrate a turbulence-induced radial fluctuation whose time scale is about 0.1 s (or even less) and length scale is 1 cm as shown in Fig. 4. In the dark center where the light intensity is very low and the gradient is also flat, this radial movement does not cause much light fluctuation experienced by a cell as it follows the trajectory. However, in the illuminated zone where the light intensity gradient is steep, the radial movement do introduce high light fluctuation experienced by the cells, called type III. As can be seen from Fig. 4, more radial fluctuations are present in the draft tube column than in the split column.

Using the ordered circulation between the riser and the downcomer in the airlift columns as basic units, the simulated cells' movement can be further analyzed statistically and quantitatively. A single trajectory is defined as one such circulation of the particle in the reactor, i.e. it starts from a given plane in the lower part of the draft tube and returns to this plane after it has traveled through the riser and the downcomer. For each CARPT experiment, more than 2000 trajectories have been identified. The circulation time distribution and the trajectory length distribution for the two airlift columns at $U_g$=5 cm s$^{-1}$, as well as the average quantity and the dimensionless variance ($\sigma$), are shown in Fig. 5. As can be seen, the split column has a faster circulation and narrower distributions than the draft tube column, indicating that its flow characteristic is closer to plug flow (i.e., less macro-mixing). This indication can be further proved by trajectory length distribution (TLD) analysis, proposed by Villermaux (1996). The macromixing index, $M$, to characterize the liquid mixing and the fluctuation, is defined as (Villermaux, 1996):

$$M = \frac{\langle l \rangle}{L}, \tag{1}$$

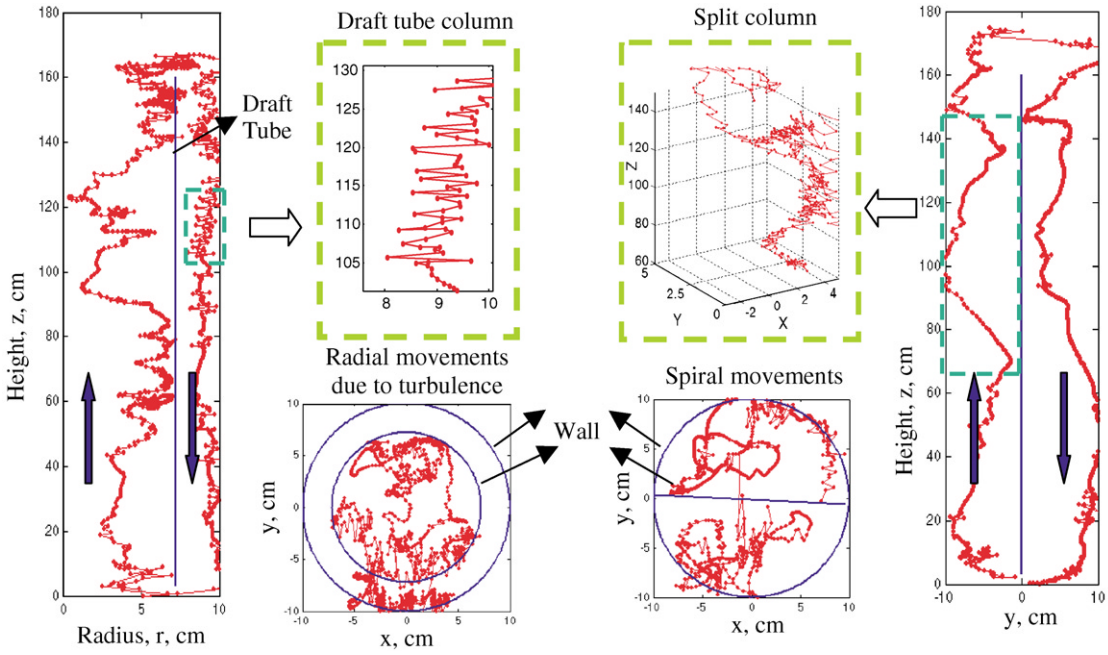


Fig. 4. Typical particle trajectories in the draft tube and the split columns. Only one recirculation is shown for each reactor, while both the front and the top view of the trajectories are shown respectively in the $r$–$z$ plane and the cross-sectional plane. Solid lines inside the figures represent the walls and internals, i.e. draft tube and split wall. $U_g = 1$ cm s$^{-1}$.

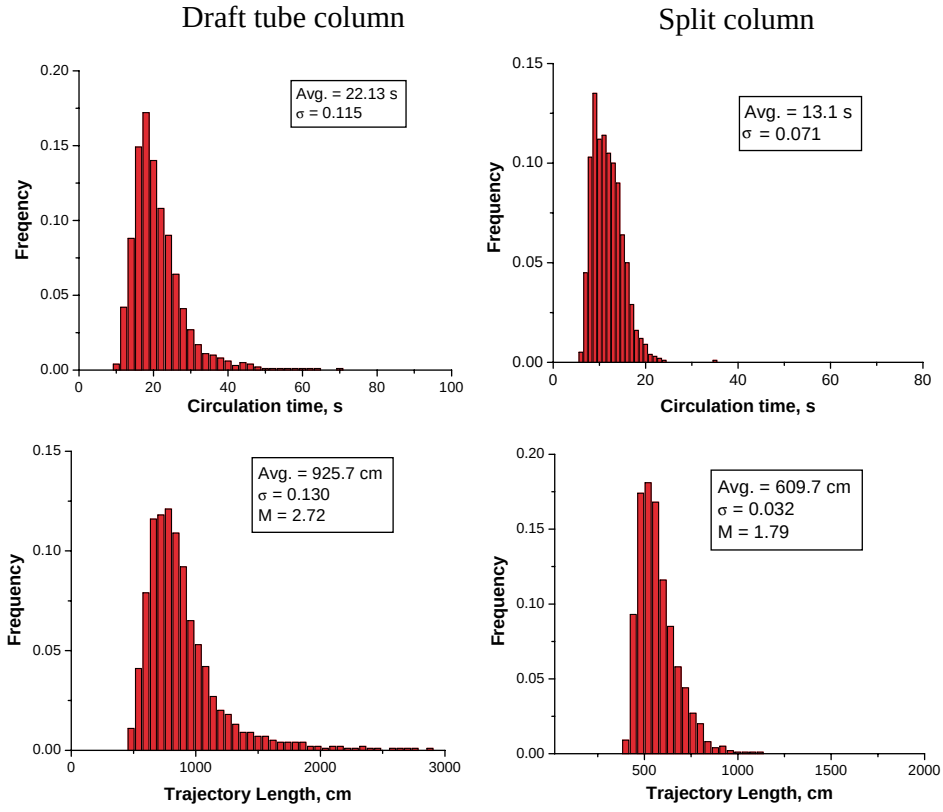


Fig. 5. Circulation time distribution and single trajectory length distribution at superficial gas velocity of 5 cm s$^{-1}$.

where $\langle l \rangle$ is the average single trajectory length and $L$ is the characteristic length of the reactor (here it is two times the reactor height, due to the recirculation). A large $M$ corresponds to very efficient macromixing, as fluid elements cover long distances with respect to the vessel size, indicating more radial variance or faster light fluctuation in PBRs.

For example, in the case of perfect mixing, $M \to \infty$, while in the case of plug flow there is no macromixing at all and thus $M = 1$. The calculated $M$ for the two airlift columns at $U_g$ of 5 cm $s^{-1}$ is also shown in Fig. 5. Again, a smaller $M$ for the split column than for the draft tube column confirmed that its flow characteristic is closer to plug flow with less radial fluctuation, which meets the observation from the particle trajectories in Fig. 4. It is noteworthy that, although the statistical analysis is based on the cells' movement, it can be easily extended to analyze other variables. For example, when applied to the temporal light pattern, it can characterize the quantity and the quality of the light exposed to the cells.

### 4.3. Temporal light pattern

One significant advantage of using CARPT for PBR analysis is the coupling of the CARPT-obtained trajectories, which represent the cells' movement, $f(x, y, z, t)$, with a suitable irradiance distribution model, which provides light intensity distribution in the reactors, $I(x, y, z)$. The temporal irradiance pattern, $I(t)$ thus yielded, represents the history of the light intensity experienced by a cell following the tracer particle trajectory. This coupling allow us to evaluate, for the first time, both the quantity and the quality of the light delivered to the cells grown in PBRs. We can analyze the total photon flux, the magnitude of the changes in irradiance, the frequencies and duration of dark periods, and the influences of reactor geometry and the operating conditions. Such information is critical for successful performance prediction and modeling, design, scale-up and operation of PBRs.

The irradiance distribution model proposed by Acien, Garcia-Camacho, Sanchez, Fernandez, and Molina (1997) was used in this work to calculate the temporal irradiance pattern. For the sake of simplicity, the external irradiance ($I_0$) is assumed to be homogeneous, which gives radial symmetry, and has a value of 1000 μE $m^{-2}$ $s^{-1}$. However, the model proposed by Grima et al. (1997) allows the calculation of the irradiance field, $I(x, y, z)$, under much more complicated and realistic conditions. The temporal irradiance patterns for a period of about 80 s, for demonstration, shown in Fig. 6, has been calculated for all the three PBRs for different biomass concentrations, assuming a constant extinction coefficient, $K_a$, of 0.05 $m^2$ $g^{-1}$.

As mentioned above, the cells experience three types of light fluctuations in the PBRs at different time scales. Type I is in the order of 10 s due to the circulation between the riser and the downcomer. Type II is in the order of 1 s due to the spiral movements. And type III is in the order of 0.1 s, or even smaller, due to turbulence. In general, the temporal irradiance pattern is influenced by biomass concentration (or the resulting optical thickness), reactor geometry, and aeration rate. These variables either affect the total photon flux or affect any of the three types of light fluctuations.

The biomass concentration ($C_b$) significantly affects the quantity of the photon flux and the magnitude of the fluctuations the cells experienced. For any type of reactor, it is clear from Fig. 6 that the total photon flux decreases considerably as the biomass concentration increases, while the magnitude of the light fluctuation increases greatly. For example, whereas the calculated irradiance ($I$) varies up to six times (100–600 μE $m^{-2}$ $s^{-1}$) at $C_b = 1000$ g $m^{-3}$, the light exposure becomes an alternation of dark/light periods in the case of a more realistic biomass concentration, 5000 g $m^{-3}$.

The reactor geometry determines the flow field that in turn determines the cells' movement and hence the light fluctuations they experienced. Its influence on the irradiance pattern can be observed partly in Fig. 6; however, further analysis to quantify such effects is needed. In Fig. 6 for the bubble column, the fluctuation of type III is prominent, but the other two types of fluctuation are difficult or impossible to be observed. While rapid irradiance changes are an advantage, the drawback of the bubble column system is that it cannot guarantee that all the cells receive frequent exposure. Unlike airlift columns, there is a lack of ordered circulation. In the split column, as mentioned above, the fluctuation of types II and III should present; however only type III is obvious from Fig. 6. The fluctuation of type II is unobserved because the spiral movement, as shown in the time-averaged velocity vector plot in Fig. 3, is rather a long time phenomenon that may not be obvious at each transient time window. As for the draft tube column, both fluctuations of types III and I are obvious from Fig. 6. It shows an ordered characteristic exposition pattern in which a fast alternation of light and darkness is followed by a long dark period. The long dark period may impair cell growth, but it is noteworthy that the time for this dark period can be adjusted by changing the relative area of the riser to the downcomer.

The time irradiance patterns in Fig. 6 also show the effects of the aeration rate. Aeration is essential in pneumatic reactors as it provides metabolite removal (oxygen), $CO_2$ transport, and agitation, which is especially indispensable in optically dense cultures. It is clear from Fig. 6 that, for any type of reactor, a higher aeration rate results in faster light fluctuation, indicating the promotion of mixing and turbulence. However, a higher aeration rate causes higher shear rates that could damage the cells.

From the above discussions, it is obvious that the irradiance pattern yield by combining the CARPT obtained Lagrangian trajectory with the irradiance model can be used to assess the effects of the operational conditions and reactor design parameters on the irradiance pattern of PBRs. However, to further analyze the effects of such irradiance patterns and their light fluctuation frequencies on bioreactor performance, one needs to quantify their effects on the mechanism of photoinhibition and photolimitation experienced in PBRs. Hence, further quantitative analysis that integrates irradiance pattern knowledge with proper

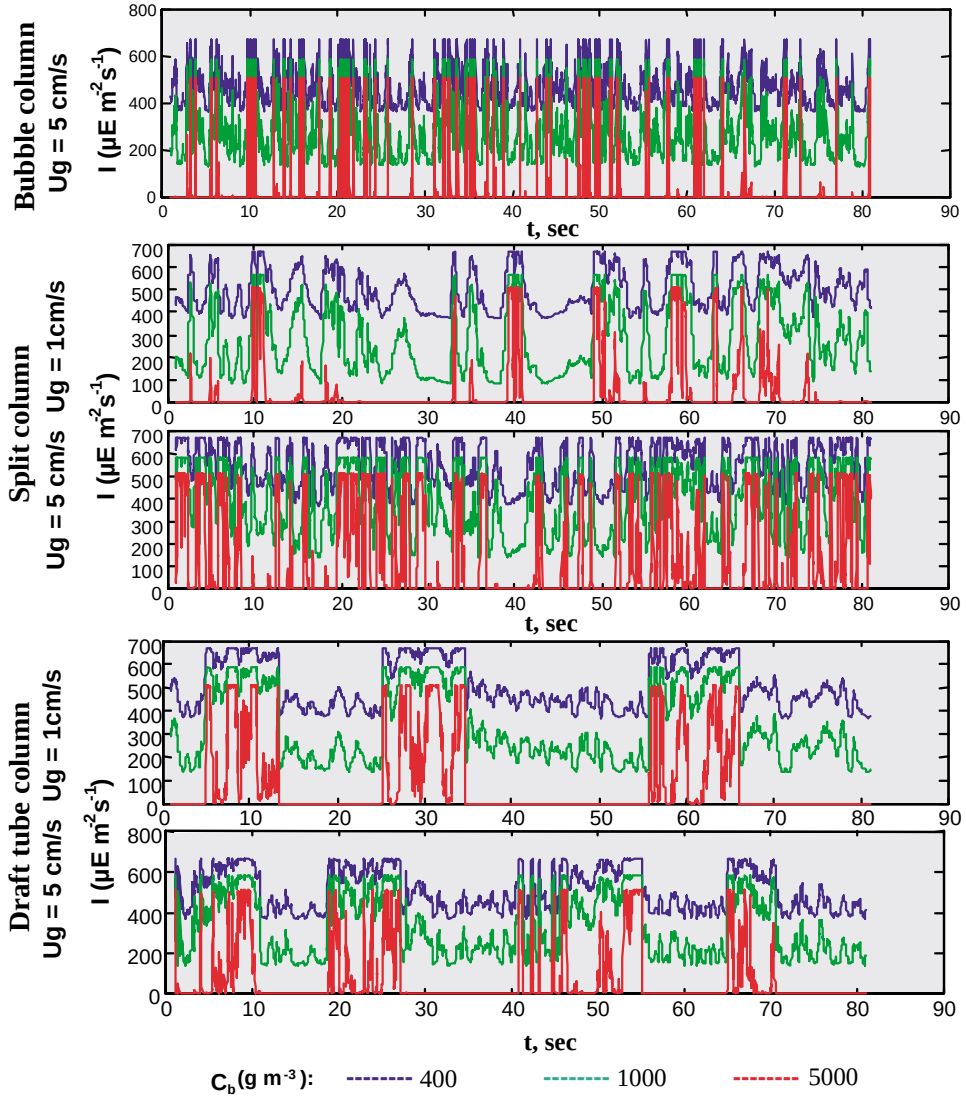


Fig. 6. Typical temporal irradiance pattern for the three PBRs at different biomass concentrations at different superficial gas velocities. Calculated by combing CARPT-obtained trajectories and the irradiance distribution model proposed by Acien et al. (1997) $K_a = 0.05$ m$^2$ g$^{-1}$.

photosynthesis models is needed to quantitatively characterize the cells' growth in PBRs. This work is in progress in our laboratory.

## 5. Remarks

In this work, the CARPT technique has been employed to determine the flow field, liquid velocity profiles, cells' movements, and the temporal irradiance patterns obtained by coupling the cells' trajectory and the irradiance distribution model. The effects of biomass concentration, reactor geometry, and the aeration rate on the irradiance patterns have been illustrated. The results indicate that the CARPT technique is promising for the PBR analysis and for obtaining fundamental information needed to advance cell growth prediction and the modeling, design, scale-up and operation of PBRs. For the first time, CARPT results allow us to investigate the effect of the studied parameters on the irradiance patterns—the controlling step of biomass productivity—both quantitatively and qualitatively.

## Notation

| | |
|---|---|
| $C_b$ | biomass concentration, g m$^{-3}$ |
| $I$ | light intensity, $\mu E$ m$^{-2}$ s$^{-1}$ |
| $I_0$ | external irradiance, $\mu E$ m$^{-2}$ s$^{-1}$ |
| $K_a$ | extinction coefficient, m$^2$ g$^{-1}$ |
| $\langle l \rangle$ | average single trajectory length, m |
| $L$ | path length of the circulation in the reactor, m |
| $M$ | micromixing indexes, dimensionless |
| $U_g$ | superficial gas velocity, cm s$^{-1}$ |

*Greek letter*

$\sigma$ dimensionless variance of PDFs

## References


Acien, F. G., Garcia-Camacho, F., Sanchez, J. A., Fernandez, J. M., & Molina, E. (1997). A model for light distribution and average solar irradiance inside outdoor tubular photobioreactors for the microalgal mass culture. *Biotechnology and Bioengineering*, *55*, 701–714.

Aiba, S. (1982). Growth kinetics of photosynthetic microorganisms. *Advances in Biochemical Engineering*, *23*, 85–156.

Barber, J., & Andersson, B. (1992). Too much of a good thing: Light can be bad for photosynthesis. *Trends in Biochemical Science*, *17*, 61–66.

Becker, E. W. (1994). Microalgae: Biotechnology and microbiology. In J. Baddiley, N. H. Carey, I. J. Higgins, & W. G. Potter (Eds.), *Studies in biotechnology, series 10*. Cambridge: Cambridge University Press.

Degaleesan, S. (1997). *Fluid dynamic measurements and modeling of liquid mixing in bubble columns*. D.Sc. Thesis, Washington University, St. Louis, MO, USA.

Devanathan, N., Moslemian, D., & Dudukovic, M. P. (1990). Flow mapping in bubble column using CARPT. *Chemical Engineering Science*, *45*, 2285–2291.

Grima, E. M., Camacho, F. G., Peres, J. A. S., Fernandez, F. G. A., & Sevilla, J. M. F. (1997). Evaluation of photosynthetic efficiency in microalgal cultures using averaged irradiance. *Enzyme and Microbial Technology*, *21*, 375–381.

Kulick, M. M. (1995). The potential for using cyanobacteria (blue-green algae) and algae in the biological control of plant pathogenic bacteria and fungi. *European Journal of Plant Pathology*, *101*, 585–599.

Kumar, S. B., & Dudukovic, M. P. (1997). Computer assisted gamma and X-ray tomography: Application to multiphase flow. In J. Chaouki, F. Larachi, & M. P. Dudukovic (Eds.), *Non-invasive monitoring of multiphase flows*. Amsterdam, The Netherlands: Elsevier.

Laws, E. A., Terry, K. L., Wichman, J., & Chalup, M. S. (1983). A simple algal production system designed to utilize the flashing light effect. *Biotechnology and Bioengineering*, *25*, 2319–2335.

Markl, H. (1980). *Modeling of algal production systems* (pp. 361–383). Amsterdam: Elsevier.

Merchuk, J. C., Ronen, M., Giris, S., & Arad, S. (1998). Light/dark cycles in the growth of the red microalga Porphyridium Sp. *Biotechnology & Bioengineering*, *59*(6), 705–713.

Pulz, O., & Scheibenbogen, K. (1998). Photobioreactors: Design and performance with respect to light energy input. *Advances in Biochemical Engineering/Biotechnology*, *59*, 123–151.

Roy, S., Larachi, F., Al-Dahhan, M. H., & Dudukovic, M. P. (2002). Optimal design of radioactive particle tracking experiments for flow mapping in opaque multiphase reactors. *Applied Radiation and Isotopes*, *56*(3), 485–503.

Rorrer, G. L., & Mullikin, R. K. (1999). Modeling and simulation of a tubular recycle photbioreactor for macroalgal cell suspension cultures. *Chemical Engineering Science*, *54*(15–16), 3153–3162.

Villermaux, J. (1996). Trajectory length distribution (TLD), a novel concept to characterize the mixing in flow system. *Chemical Engineering Science*, *51*, 1939–1946.

Vonshak, A. (1992). Microalgal biotechnology: Is it an economic success? In E. J. Da SilVa, C. Ratledge, & A. Sasson (Eds.), *Biotechnology: Economic and social aspects, issue for developing countries.* Cambridge: Cambridge University Press.